SAND2014-17791J

Rapid first-cycle lithiation strategy for enhanced performance of Li-MoS_2 batteries as identified by *in situ* studies

Jiayu Wan,[(a),1] Wenzhong Bao,[(a),1,2] Yang Liu[(a),3], Jiaqi Dai[1], Fei Shen[1], Lihui Zhou,[1] Xinghan Cai[2], Dan Urban[1], Yuanyuan Li[1], Katherine Jungjohann,[3] Michael S. Fuhrer*[2,4], Liangbing Hu*[1]
1 Department of Materials Science and Engineering, University of Maryland, College Park, MD 20742-4111, USA.
2 Department of Physics, University of Maryland, College Park, MD 20742-4111, USA.
3 Center for Integrated Nanotechnologies (CINT), Sandia National Laboratories, Albuquerque, New Mexico 87185, United States
4 School of Physics, Monash University, Victoria 3800, Australia.
*Corresponding Authors: binghu@umd.edu, michael.fuhrer@monash.edu
(a) These authors contribute equally to this work

Abstract

Layer-structured materials with van der Waals gaps have long been utilized as active electrode materials in rechargeable Li ion batteries. However, understanding of their nanostructure and associated property changes during charging/discharging process is lacking. We developed a novel planar nanobattery platform that allows us to measure *in situ* electrical transport and optical properties of two-dimensional (2D) molybdenum disulfide (MoS_2) at the level of individual crystallites a few microns in extent along the basal plane, and a few nanometers in thickness. We observe a large conductivity increase of thick MoS_2 crystallites only at rapid charging rate during the first lithiation cycle due to the formation of a percolative Mo nanoparticle network imbedded in Li_2S matrix, which is confirmed by *in situ* transmission electron microscopy. The nanoscale study leads us to develop a novel charging strategy for Li-ion batteries: rapid charging in the first cycle can largely improve the capacity and cycling performance confirmed in bulk MoS_2/Li coin cells. The proposed nanobattery methodology can be generally applied to study a range of 2D electrochemical materials at the nanoscale.

Key Words

MoS_2 nanoflake, rapid lithiation, nanobattery, *in situ* transport, *in situ* TEM, optical transmittance

Introduction

MoS_2 is an earth-abundant mineral material that has been widely studied for its many applications such as lubrication, hydrodesulfurization catalysis, and as an electrical energy storage electrode.(1-3) Recently, two dimensional (2D) MoS_2 crystals have attracted tremendous research interest for their unique properties in photonics, optoelectronics, electrics and energy applications.(4-12) Liquid phase exfoliation of layered materials can provide an excellent approach for mass production of 2D materials, (13-15) enabling applications which require a large quantity of materials, particularly electrical energy storage. Indeed the large van der Waals gap of MoS_2 enables excellent electrochemical performance, and MoS_2-based Li-ion, Na-ion, and Mg-ion batteries are being explored for electric vehicles and grid-scale storage.(16-21)

Battery electrode materials are complex composites with structure at several length scales, being composed of active materials (e.g. MoS_2), conductive additives (e.g. carbon black), and binders (e.g. polyvinylidene difluoride). Conventional electrochemical characterization techniques, such as cyclic voltammetry (CV), galvanostatic intermittent titration technique (GITT), electrochemical impedance spectroscopy (EIS), etc. reveal the performance of the bulk composite electrode, but cannot probe the intrinsic properties of the active material itself during ion insertion. Recent *in situ* TEM studies of nanostructured electrodes have partially overcome this, successfully observing the structural changes during the charge/discharge process, (22) leading to a better understanding of mechanical properties and kinetics, and thus a better electrode design. Still, information about the electronic structure of the active material, and its intrinsic electronic transport properties, which are at least equally important in making better batteries, is still lacking.

We have designed a planar nanobattery that allows *in situ* electrical transport measurement during electrochemical charge and discharge in micron-sized individual crystallites of 2D layered nanosheets, as well as optical studies (transmittance, Raman spectroscopy), which can give information about the electronic structure of the active material. To demonstrate the utility of our nanobattery platform, we study the lithiation of MoS_2 crystallites. We observe that the electrical conductivity of the 2D MoS_2 crystallites is highly dependent on thickness and the rate of lithiation in the first cycle. We use *in situ* TEM to confirm that upon rapid first-cycle lithiation the formation of a Mo conductive network imbedded in the Li_2S matrix leads to an enhanced electrical conductivity compared to the pristine MoS_2. We applied the results in Li-MoS_2 coin cells with composite electrodes, demonstrating that batteries with fast lithiation on the first cycle showed significantly higher specific capacity than batteries lithiated slowly. The nanobattery platform can be generally applied to other energy storage materials and a wide range of characterization techniques, and is thus a powerful tool to uncover the properties of nanoscale materials undergoing electrochemical modification. As in the example demonstrated here, we expect this platform will lead to new insights into the operation of battery materials at the nanoscale, leading to new strategies in improving the cell performance.

Results

Nanobattery for *in situ* measurement A schematic crystal structure of 2H MoS_2 is illustrated in **Fig 1A**, with the lattice parameters a = 3.16 Å and c = 12.29 Å. Our nanobattery developed for the *in situ* measurement of the optical transmittance and electronic transport of 2D nanomaterials is illustrated in Fig. 1B. A MoS_2 crystal and lithium metal are deposited on top of the Cu transport electrodes and current collector respectively. The MoS_2 flake can be charged/discharged by connecting transport electrodes and current collector to an

electrochemical workstation. Coupling the nanobattery with a transmission optical microscope/probe station, we can then carry out *in situ* optical transmittance and electronic transport measurements on the same MoS_2 crystal. Optical images of uniform-thickness mechanically exfoliated MoS_2 crystals are shown in Figs. 1C and D, with dimensions as large as 100 μm × 100 μm. We used atomic force microscopy (AFM) to determine the morphology and thickness of exfoliated MoS_2, in Figs. 1E and 1F. A photograph of the complete nanobattery device is shown in Fig. 1G. The region of the transport electrodes is expanded in Fig. 1H, showing a large uniform area of MoS_2 crystal spanning the electrodes.

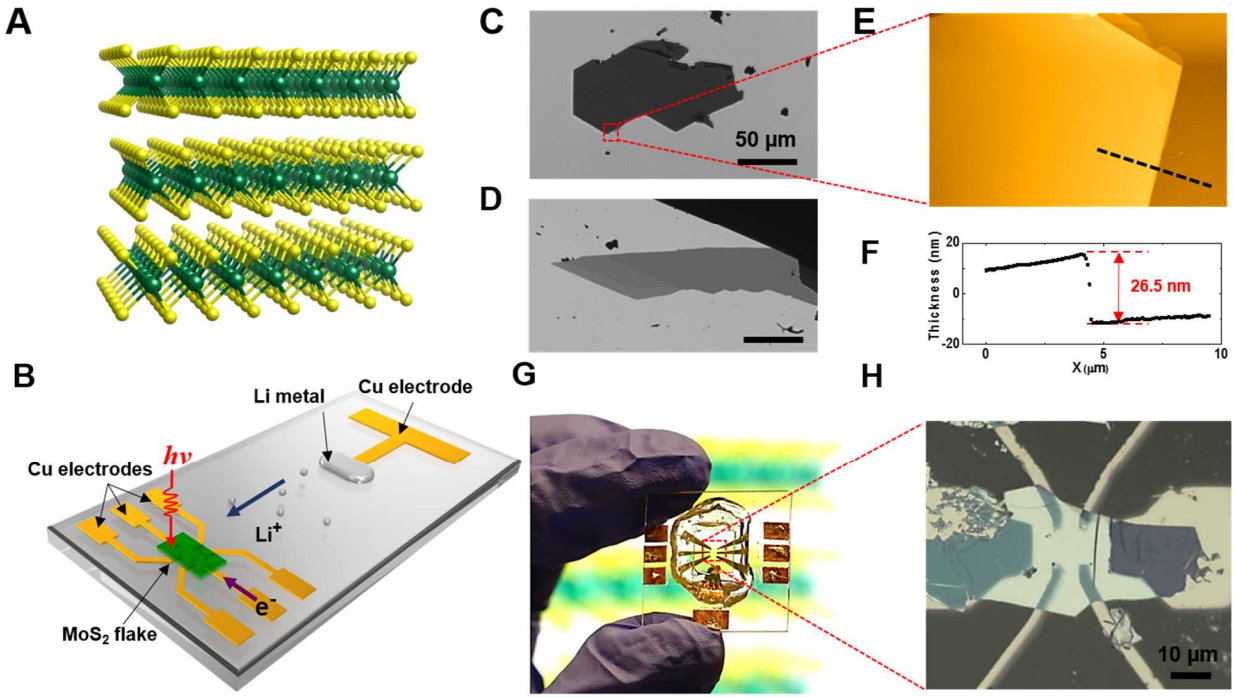

Figure 1 Li-MoS_2 nanobattery. (A) Lattice structure of 2H-MoS_2. (B) Schematic of MoS_2-Li nanobattery. (C), (D) Optical images of large area uniform MoS_2 crystals on glass substrates at 550 nm wavelength under transmission mode; both scale bars are 50 μm. (E) AFM image of MoS_2 crystal in (C). (F) Line trace of AFM image along dashed line in (E). (G) Photograph of nanobattery. (H) Micrograph of electrode area with MoS_2.

Electronic transport To understand the intrinsic resistance change during lithiation, an *in situ* electrical transport measurement was carried out using our nanobattery setup. Fig. 2A shows the simultaneously measured resistance and electrochemical potential at small constant lithiation current at 0.5 uA for a single MoS_2 crystal of thickness 35 nm. **Fig 2A** inset illustrates the experimental setup; the MoS_2 crystal in the nanobattery was lithiated at a constant current, while the electrochemical potential and 4-probe electrical resistance of the crystal were monitored. During the first cycle of lithiation, three reactions occur:

$$xLi + 2H\text{-}MoS_2 \rightarrow 2H\text{-}Li_xMoS_2 \ (0 \leq x \leq 0.1) \quad (1)$$

$$yLi + 2H\text{-}Li_x\ MoS_2 \rightarrow 1T\text{-}Li_{x+y}MoS_2 \ (0.1 \leqslant x + y \leqslant 1) \quad (2)$$

$$3Li + 1T\text{-}LiMoS_2 \rightarrow Li_2S + Mo \quad (3)$$

We identify these three reactions with the regions marked I, II, and III respectively in Fig. 2A. In region I, we observe a rapid decrease of the electrochemical potential, and a rapid decrease and rise of the resistance. We interpret this as the region where reversible Li intercalation of the Van de Waals gaps of 2H-MoS_2 occurs with little lattice distortion [Eqn. (1); $0 < x < 0.1$](2). With increasing concentration of Li, a reversible phase change occurs from 2H-Li_xMoS_2 to 1T-Li_xMoS_2 corresponding to Eqn (2), and is marked by a clear plateau of ~1.1 V. The resistance in region II is always lower than the initial resistance, consistent with the formation of the metallic 1T-$Li_{x+y}MoS_2$ phase. The completion of Eqn. 2 at 1T-$LiMoS_2$ marks the end of region 2. Region 3 shows another clear plateau in at ~ 0.6 V, corresponding to Eqn. (3), the conversion reaction from 1T-$LiMoS_2$ to Li_2S and Mo metal. The resistance jumps abruptly at the onset of region III, consistent with the formation of the insulating matrix, and stays always higher than the initial resistance of the pristine MoS_2.

Importantly, qualitatively different behavior of the resistance is observed in the same setup upon rapid discharging, accomplished by shorting the Li electrode to the MoS_2 electrode to promote rapid insertion of Li into MoS_2. A large overpotential between the two electrodes enables a rapid formation of Mo and Li_2S. Fig. 2B shows the time profile of the resistance for a shorted MoS_2 crystal (thickness 46 nm); a schematic of the measurement setup is shown in Fig 2B inset. In contrast to slow discharging (Fig. 2A), here a drastic decrease in the resistance within a few minutes was observed of over 3 orders of magnitude, from 5×10^5 to 190 ohms. After shorting for 24 hours the resistance stayed the same, which suggested the low resistance is associated with the MoS_2 reaction products and not due to Li plating (also no Li plating was observed optically). After the nanobattery was disconnected for 36 hours, the resistance increased only a little to 210 ohms, which indicated the high stability of the final product. The process was repeated for many MoS_2 crystals of different thicknesses with results shown in Fig. 2C. Strikingly, we observe a thickness dependent relationship on the final resistance of the Li-inserted MoS_2. For pristine MoS_2 crystals of thickness greater than 30 nm, a drastic resistance drop occurred after lithiation. However, with thinner crystals, an increase in the resistance was observed, of magnitude similar to that observed for slow lithiation (Fig. 2A).

Since we expect that in all cases the final product of lithiated MoS_2 is Mo nanoparticles and Li_2S,(24) the complexity of resistance change suggests that the morphology and connectivity of the nanostructured Mo may change with different lithiation rates. We hypothesize that slowly lithiated MoS_2 forms isolated Mo nanoparticles which do not enhance the conductivity, thus the resistance is dominated by the insulating Li_2S (Fig. 2D) while upon rapid lithiation of thick MoS_2, Mo nanoparticles form a percolating metallic network, enhancing the conductivity (Fig. 2E).

Thinner MoS_2 always shows more resistive behavior, and we suppose this is due to the difficulty of forming a percolating network in a thin sample (Fig. 2F).

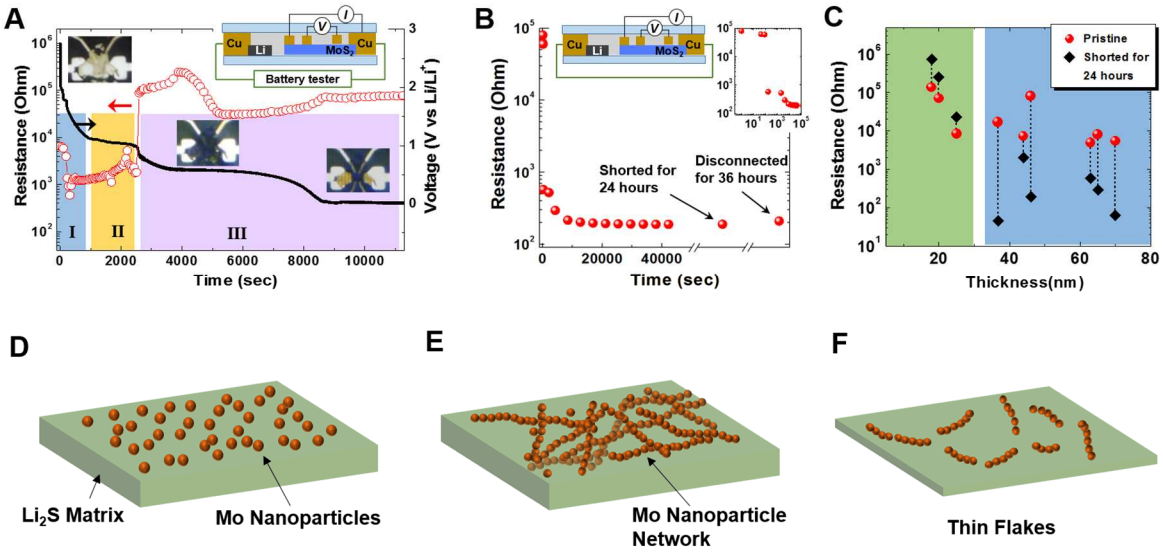

Figure 2. Electronic transport measurement. (A) Resistance vs. time of MoS_2 flake undergoing electrochemical lithiation at constant current. Insets show a schematic of the nanobattery setup for *in situ* resistance measurement (upper right), and optical images of lithiated MoS_2 at stages I, II, and III, from left to right. (B) Resistance vs. time for a MoS_2 crystal after electrically shorting the nanobattery. Insets show a schematic of the nanobattery for *in situ* resistance measurement during shorting, and a log-log plot of the resistance vs. time. (C) Resistance vs. thickness phase diagram of shorted MoS_2 crystals; red circles show resistance of pristine MoS_2, black diamonds show resistance after shorting of nanobattery. (D) Schematic showing discontinuous Mo particles imbedded in Li_2S matrix resulting from slow lithiation in thick MoS_2. (E) Schematic showing percolative Mo nanoparticle network imbedded in Li_2S matrix resulting from fast lithiation in thick MoS_2. (F) Schematic of discontinuous Mo particle network imbedded in Li_2S matrix resulting from fast lithiation in thin MoS_2 crystallite.

In order to confirm our hypothesis that charging rate-dependent Mo nanostructure determines the conductivity of MoS_2 after lithiation, we used transmission electron microscopy (TEM) with *in situ* electrochemistry to determine the structure of the final product. **Fig. 3A** illustrates the principle of the *in situ* electrochemical TEM setup. MoS_2 flakes obtained from liquid exfoliation (14) were attached to an Au rod, serving as the working electrode. Li metal was attached to a W rod, serving as the counter and reference electrodes. A thin layer of native

oxide Li_2O was formed during the transfer process and acted as the solid-state electrolyte for Li ion transport. The Li/Li_2O electrode was controlled by nano-manipulator inside the TEM, and made contact with the selected MoS_2 nanoflake (also see Figure S1). Fig 3B shows a bright-field TEM image of a pristine MoS_2 crystallite attached to the Au electrode. Fig 3C shows the diffraction pattern of the MoS_2. The diffraction spots marked in red circles show a 6-fold symmetry and correspond to the 2H crystal structure of MoS_2. Additional diffraction spots correspond to additional MoS_2 crystals with different rotational orientations. Fig. 3D shows a high-resolution TEM (HRTEM) image of pristine MoS_2, clearly showing in which the periodic triangular lattice of Mo atoms is resolved. The Mo-Mo distance is 0.27 nm as expected for 2H-MoS_2.

In the *in situ* electrochemical TEM experiment, the lithiation process is controlled by the voltage difference between the two electrodes. When a large voltage difference of -2 V was applied on the MoS_2 electrode against the Li counter electrode, the lithiation process started. After full lithiation, a large volume expansion resulted in a curving flake compared to the pristine MoS_2, shown in Fig. 3E. The corresponding diffraction pattern (Fig. 3F) indicates the formation of polycrystalline Li_2S and a very fine Mo metal nanostructure in the final product. From the HRTEM image of the final product as shown in Fig. 3G, the dark contrast corresponds to Mo nanoparticles with diameter about 1 nm, which can be seen to form a continuous network that we believe provides the electron transport pathway within the insulating Li_2S matrix. (Also see Figure S2) This observation confirms our explanation of the reduction in the resistance of the fully lithiated MoS_2 flakes after shorting. The formation of Mo nanoparticles can be explained by the non-equilibrium process with a large over-potential, where the nucleation of Mo nanoparticles occurs rapidly, with limited time for growth and ion diffusion. This may also

partially be the result of the low diffusivity of Mo atoms, similar to Fe in the case of FeF_2 lithiation recently reported (25). The formation of conductive paths by metal nanoparticles after lithiation has also been reported in RuO_2,(26) FeF_2 (25)and NiO(27).

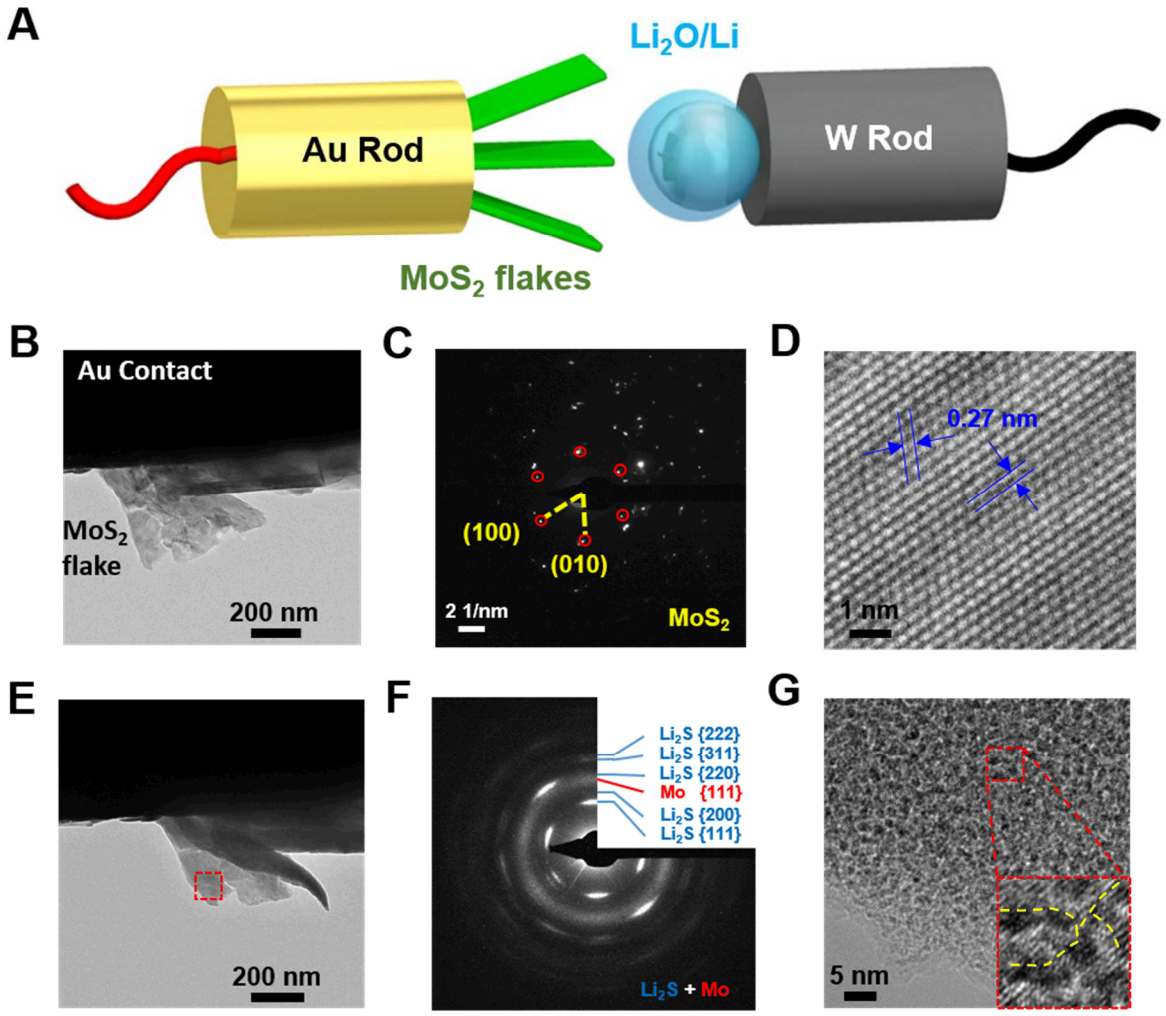

Figure 3. *In situ* TEM of MoS_2 lithiation. (A) Schematic illustration of *in situ* TEM nanobattery setup. (B) Pristine MoS_2 nanoflake attached on Au substrate. (C) Electron diffraction pattern of pristine MoS_2, the spots circled by red correspond to the 2H crystal structure of MoS_2. (D) HRTEM of the MoS_2 flake showing lattice constant of 0.27 nm. (E) TEM of final product after full lithiation. (F) Electron diffraction pattern of final product. Rings in the diffraction pattern correspond to randomly oriented crystallites; the corresponding crystal indices for Mo and Li_2S are indicated in the legend. (G) HRTEM image of the final product.

***In situ* Optical transmittance measurement** An *in situ* optical transmittance measurement was also made during lithiation of MoS_2 using with the nanobattery setup, as illustrated in **Fig. 4A**. Figs. 4B-D show the optical images of a MoS_2 crystal under 450 nm wavelength at potentials of 2.8 V, 0.9 V, and 0.05 V (vs. Li^+/Li). With increasing lithiation, these three typical images clearly show an increase in the transmittance of the crystal. This is further depicted in Fig 4E where the optical transmittances of a crystal (blue dots, 7.9 nm;) were monitored as a function of time simultaneous to the electrochemical potential (black line) as lithiation proceeded with a constant current. Again we denote the three different regions in electrochemical potential as I, II, III. Here we see that each region corresponds well to a plateau in optical transmission, as can be seen in Fig 4E. In region I, a slightly increase of transmittance is observed as Li intercalated into MoS_2 (before 2500 s). From region I to region II, a sudden increase of transmittance occurred, corresponding to a phase transition from 2H to 1T upon Li insertion. At the end of the second plateau (~12500 s), we observe a graduate increase of transmittance from 65% to 80%, indicate a conversion reaction from 1T-$LiMoS_2$ to Li_2S plus Mo. The delay of the transmittance change relative to the voltage profile from region II to region III is due to kinetic limitation, result from the high resistance of the 1T-$LiMoS_2$/Li_2S+Mo flake, with a thickness of 7.9 nm.

Fig 4F shows the wavelength dependent transmittance of each stage. Stage I shows a typical wavelength dependence for pristine MoS_2 crystals.(28, 29) Stage II shows increased transmittance at shorter wavelengths (less than 700 nm), and decreased transmittance at longer wavelengths, compared to the pristine MoS_2. The final product, after region III, corresponding to Li_2S and Mo metal, shows higher transmittance than MoS_2 at all measured wavelength (400 nm – 800 nm). We investigated a wide thickness range of MoS_2 crystals, all showed an increase of transmittance after lithiation. While more work is needed to understand the details of the

transmittance spectra, the changes in optical properties during electrochemical lithiation are qualitatively as expected for the structure changes as discussed above. While MoS_2 has a bandgap in the visible range with limited transmittance, reaction product Li_2S is insulating and expected to be fairly transparent. The percolative Mo network is also fairly transparent due to the small thickness.

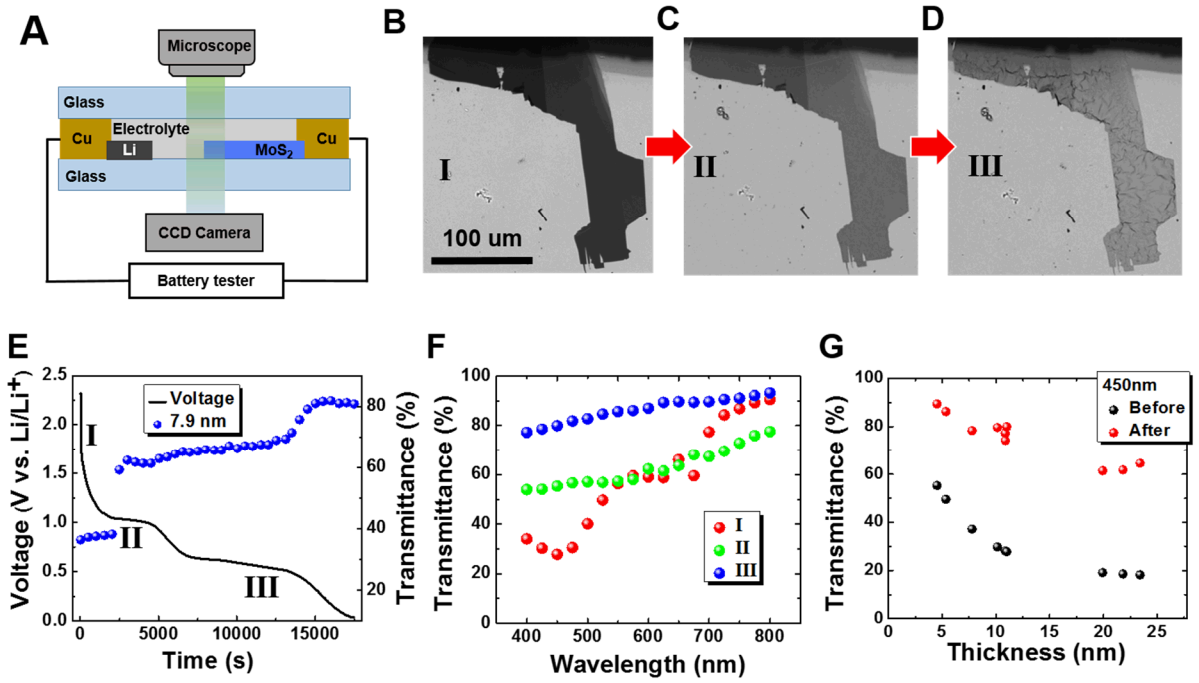

Figure 4 *In situ* optical transmittance measurement. (A) Schematic of *in situ* optical transmittance measurement of MoS_2 lithiation. (B-D) Optical images of a MoS_2 flake at 2.8 V, 0.9 V and 0.05 V. (E) Transmittance of MoS_2 flake *vs.* Li insertion voltage. (F) transmittance *vs.* wavelength for lithiated MoS_2 at three different stages. (G) Thickness dependence of transmittance of MoS_2 flakes before and after lithiation.

Coin cell measurement with MoS_2 composites Our nanobattery measurement scheme can provide crucial information for the development of macroscopic batteries. In the case discussed here, the formation of a conducting Mo nanoparticle network has significant implications for sulfur-based batteries. After the first lithiation cycle, our system corresponds to a Li-S battery with Mo nanoparticles,(1) and we expect that the formation of the percolated conductive network

can improve the storage and cycling performance by increasing the electrical connectivity of the insulating Li_2S. In order to verify the contribution of the Mo nanoparticle percolative network on the electrochemical performance of Li-MoS_2 batteries, we constructed coin cells using MoS_2/nanocellulose fiber (NFC)/Carbon Nanotube (CNT) (w:w:w = 8:2:2) composite free standing film and lithium metal as electrode materials. Here, NFC serves as a binder, and CNT as a mechanical scaffold and conductive additive in the thin film electrode. After cell assembly, two groups of cells were cycled by electrochemical workstation at constant and identical current rate. In the experimental group, before constant current cycling, we performed a first rapid lithiation by shorting the cells, which we expect to form a conductive Mo network. The control group was cycled as regular batteries at constant current, with no rapid lithiation in the first cycle. The cycling performance of two typical coin cells from each group is shown in **Fig. 5A**. Both coin cells shows a steady cycling performance for 100 cycles. However the experimental group shows a higher specific capacity than the control group at same current densities. The first 30 cycles of the two cells were cycled at 50 mA/g, where the next 70 cycles at 250 mAh/g. The experimental group (charged rapidly in the first cycle) shows a higher capacity (900 mAh/g) than control battery (800 mAh/g) at low rate, with the difference becoming much larger at high charging rate (500 mAh/g compared to 150 mAh/g). Fig. 5B shows typical voltage profiles of two cells at 250 mAh/g. The plateaus at ~2.2V (delithiation) and ~2.0V (lithiation), characterize the MoS_2 coin cells after 1^{st} cycle. Again, the experimental group not only shows a much larger capacity, but also a smaller voltage drop after 30 s of rest. Fig. 5C shows the specific capacity of an experimental group coin cell charged/discharged at different current densities. A high specific capacity of 1100 mAh/g is demonstrated at a low current density (50 mA/g) with the composite electrode. At high current density (500 mA/g), a high specific capacity of about 400 mAh/g is

still maintained, demonstrate a great promise of MoS_2 as a cathode material for Li ion batteries. All these results are consistent with a lower internal electrical resistance which provides higher capacity at high power, supporting our hypothesis that the Mo conductive network formed by the first rapid charge provides an electron pathway inside each nanoscale Li_2S/Mo flake. The results demonstrate the power of *in situ* techniques for understanding the structural and electronic changes in electrode materials undergoing electrochemical reactions, and the use of that understanding to improve battery performance. We expect that the *in situ* techniques here will be applied to study a range of phenomena in other conversion electrode materials, with the outcomes used to improve the corresponding battery technologies.

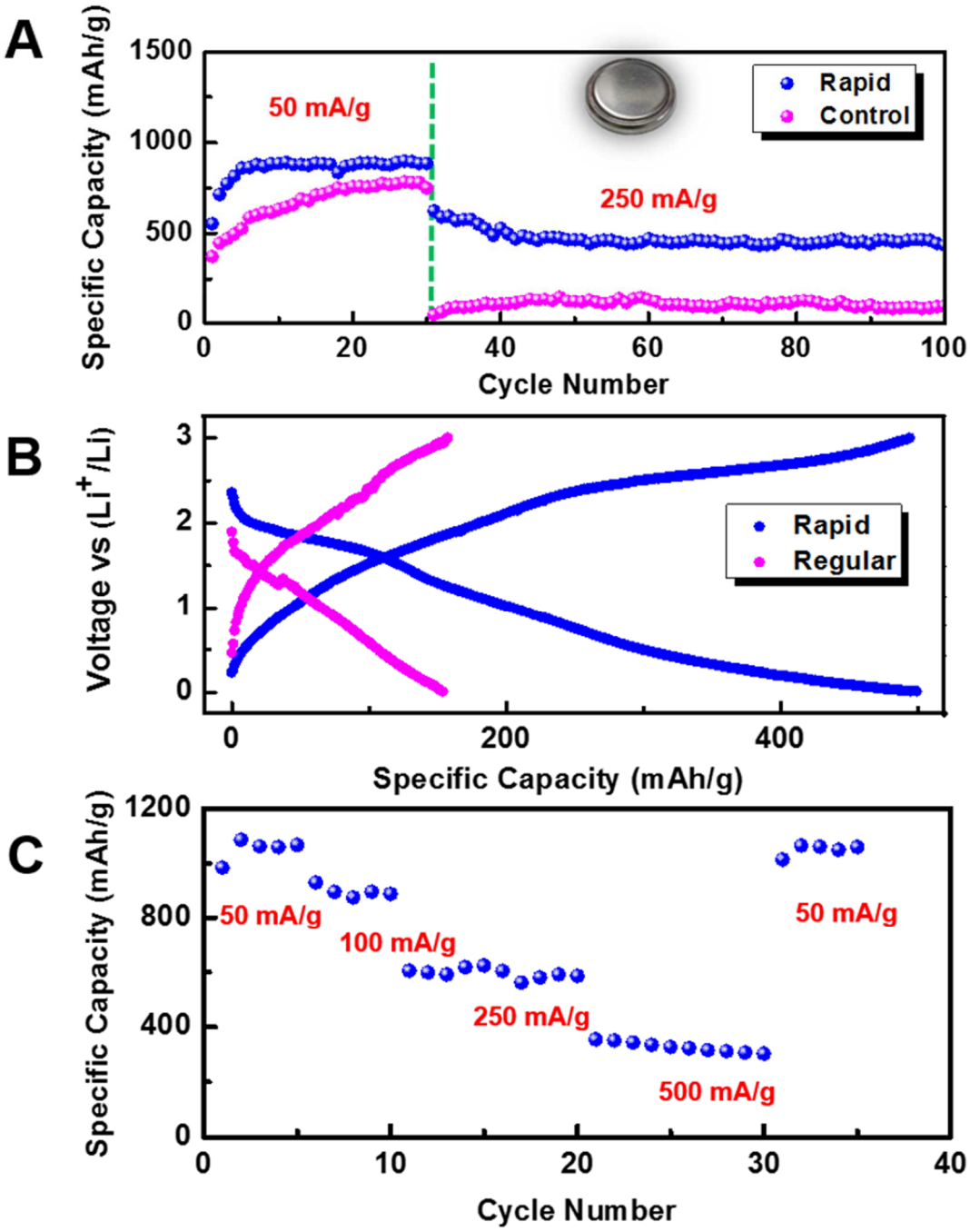

Figure 5. (A) Cycling performance (at 50 mA/g for 30 cycles and 250 mA/g for 70 cycles) of MoS_2/NFC/CNT Li ion batteries at different initial lithiation conditions. Inset is a coin cell. (B)

Voltage profile of two types of coin cells at 15th cycle. (C). Initial rapid charged coin cells cycle at different charge/discharge current density.

Conclusion

In summary, we have applied *in situ* nanobattery techniques to observe the changes in electrical resistance, optical transmission, and nanoscale structure of MoS_2 upon electrochemical lithium insertion. We observe the formation of an interconnected Mo nanoparticle network after rapid lithiation of thick MoS_2 crystals, which achieves a simultaneous increase of optical transmittance and electrical conductivity compared to pristine MoS_2. Our *in situ* investigation of lithiation at the scale of single MoS_2 crystals guided the design of higher performing Li-MoS_2 coin cell batteries, where we demonstrated a threefold increase in capacity after rapid lithiation on the first cycle compared to cells which underwent a conventional constant-current discharge. We are the first to propose and confirm the battery performance improvement by such a new charging strategy in the first cycle, which is possible based on the fundamental studies at the nanoscale.

Methods

Nano battery fabrication for *in situ* electrochemical/optical/resistance measurements. In optical transmission measurements, thin pristine MoS_2 crystals are obtained by mechanical exfoliation of bulk MoS_2 (SPI supplies) onto 0.2 mm thick glass substrates (Fisher Scientific). Cu electrodes (50 nm thickness) are then deposited on top of selected MoS_2 sheets using a shadow mask technique(30) in an electron beam evaporator. For resistance measurements, Hall bar electrodes are pre-deposited on glass substrates, and mechanically exfoliated MoS_2 crystals are then transferred onto the electrodes. This avoids mechanical damage to crystals and electrodes contact due to the volume expansion during lithiation process. Thicknesses of the

MoS_2 crystals are determined by atomic force microscopy. The devices are then transferred into an argon filled glove box, adding lithium pellet as an negative electrode and $LiPF_6$ in EC:DEC (v:v = 1:1) as electrolyte. Finally the planar battery region with electrolyte/lithium/MoS_2 is covered by another piece of 0.2 mm thick glass and sealed by polydimethylsiloxane.

MoS_2 ink preparation MoS_2 power (Sigma, 98%) is mixed with co-solvent of deionized water, ethanol/IPA at 3mg/mL. The mixture was bath sonicated for 3~7 hours for liquid exfoliation of bulk MoS_2 to thin layers of MoS_2, as shown in Fig. 3B.

***In situ* optical/resistance measurement experiment** Planar nanobatteries were fabricated and connected to a battery tester (Biologic SP150) and charged/discharged with a constant current. The optical transmittance was determined by analysis the optical images of the lithiated flakes under an optical microscope in transmission mode. *In situ* resistance measurement is carried out using a standard four-probe method during the lithiation process.

***In situ* TEM electrochemistry experiment**

The Li metal is scratched off a freshly cut surface of bulk Li with a tungsten (W) rod in a helium-filled glove box (H_2O and O_2 concentration below 1 ppm), serving as the counter electrode and Li source. Both the MoS_2 electrode and Li metal electrode are mounted onto a Nanofactory TEM-STM holder inside the same glove box and sealed in a plastic bag filled with dry helium. The holder is quickly transferred into the TEM (FEI Tecnai F30) column with exposure time to air of about 2 seconds, forming a native Li_2O layer which serves as a solid-electrolyte for Li ion transport. The Li_2O/Li electrode is driven to contact with the selected MoS_2 nanoflakes using the nano-manipulator inside the TEM, constructing a nanobattery.(31)

Coin cell materials preparation and assembly

MoS_2/NFC/CNT composite electrodes are prepared in a three-step process. First, MoS_2/NFC ink is prepared by ultrasonication of MoS_2/NFC in DI water. Single-walled CNT (P3, Carbon Solutions Inc.) is then added to the MoS_2/NFC ink and a well dispersed solution with MoS_2/NFC/CNT is obtained. Finally, the composite ink is vacuum filtrated to a free standing film. CR2032 coin cells are assembled from composite electrodes, separators, liquid electrolyte ($LiPF_6$ in EC:DEC w:w = 1:1), Li metal and coin cell components.

Acknowledgements

L. Hu acknowledge the startup support from University of Maryland and College Park. The work is also supported by the U.S. ONR MURI program. We acknowledge the support of the Maryland Nanocenter and its Fablab and its Nisplab. M.S. Fuhrer acknowledges support from an ARC Laureate Fellowship. The work was performed in part with the TEM capability supported by the Center for Integrated Nanotechnologies (CINT), an Office of Science User Facility operated for the U.S. Department of Energy (DOE) Office of Science. Sandia National Laboratories is a multiprogram laboratory managed and operated by Sandia Corporation, a wholly owned subsidiary of Lockheed Martin Corporation, for the U.S. Department of Energy's National Nuclear Security Administration under contract DE-AC04-94AL85000.

Reference

1. Stephenson T, Li Z, Olsen B, & Mitlin D (2014) Lithium ion battery applications of molybdenum disulfide (MoS2) nanocomposites. *Energy & Environmental Science* 7(1):209-231.
2. Py MA & Haering RR (1983) STRUCTURAL DESTABILIZATION INDUCED BY LITHIUM INTERCALATION IN MOS2 AND RELATED-COMPOUNDS. *Canadian Journal of Physics* 61(1):76-84.
3. Dominko R*, et al.* (2002) Dichalcogenide nanotube electrodes for Li-ion batteries. *Advanced Materials* 14(21):1531-1543.
4. Butler SZ*, et al.* (2013) Progress, Challenges, and Opportunities in Two-Dimensional Materials Beyond Graphene. *Acs Nano* 7(4):2898-2926.

5. Novoselov KS, *et al.* (2005) Two-dimensional atomic crystals. *Proceedings of the National Academy of Sciences of the United States of America* 102(30):10451-10453.
6. Wang QH, Kalantar-Zadeh K, Kis A, Coleman JN, & Strano MS (2012) Electronics and optoelectronics of two-dimensional transition metal dichalcogenides. *Nature Nanotechnology* 7(11):699-712.
7. Wang H, *et al.* (2013) Electrochemical tuning of vertically aligned MoS2 nanofilms and its application in improving hydrogen evolution reaction. *Proceedings of the National Academy of Sciences of the United States of America* 110(49):19701-19706.
8. Mak KF, He K, Shan J, & Heinz TF (2012) Control of valley polarization in monolayer MoS2 by optical helicity. *Nature Nanotechnology* 7(8):494-498.
9. Zeng H, Dai J, Yao W, Xiao D, & Cui X (2012) Valley polarization in MoS2 monolayers by optical pumping. *Nature Nanotechnology* 7(8):490-493.
10. Splendiani A, *et al.* (2010) Emerging Photoluminescence in Monolayer MoS2. *Nano Letters* 10(4):1271-1275.
11. Mak KF, Lee C, Hone J, Shan J, & Heinz TF (2010) Atomically Thin MoS2: A New Direct-Gap Semiconductor. *Physical Review Letters* 105(13).
12. Wang Y, *et al.* (2013) Electrochemical Control of Photoluminescence in Two-Dimensional MoS2 Nanoflakes. *Acs Nano* 7(11):10083-10093.
13. Zeng Z, *et al.* (2011) Single-Layer Semiconducting Nanosheets: High-Yield Preparation and Device Fabrication. *Angewandte Chemie-International Edition* 50(47):11093-11097.
14. Nicolosi V, Chhowalla M, Kanatzidis MG, Strano MS, & Coleman JN (2013) Liquid Exfoliation of Layered Materials. *Science* 340(6139):1226419.
15. Chhowalla M, *et al.* (2013) The chemistry of two-dimensional layered transition metal dichalcogenide nanosheets. *Nature Chemistry* 5(4):263-275.
16. Xiao J, *et al.* (2010) Exfoliated MoS2 Nanocomposite as an Anode Material for Lithium Ion Batteries. *Chemistry of Materials* 22(16):4522-4524.
17. Bindumadhavan K, Srivastava SK, & Mahanty S (2013) MoS2-MWCNT hybrids as a superior anode in lithium-ion batteries. *Chemical Communications* 49(18):1823-1825.
18. David L, Bhandavat R, & Singh G (2014) MoS2/Graphene Composite Paper for Sodium-Ion Battery Electrodes. *ACS Nano* 8(2):1759-1770.
19. Park J, *et al.* (2013) Discharge mechanism of MoS2 for sodium ion battery: Electrochemical measurements and characterization. *Electrochimica Acta* 92:427-432.
20. Liang Y, *et al.* (2011) Rechargeable Mg Batteries with Graphene-like MoS2 Cathode and Ultrasmall Mg Nanoparticle Anode. *Advanced Materials* 23(5):640-643.
21. Liu Y, *et al.* (2013) Sandwich-structured graphene-like MoS2/C microspheres for rechargeable Mg batteries. *Journal of Materials Chemistry A* 1(19):5822-5826.
22. Liu XH, *et al.* (2011) Anisotropic Swelling and Fracture of Silicon Nanowires during Lithiation. *Nano Letters* 11(8):3312-3318.
23. Tonti D, Pettenkofer C, & Jaegermann W (2004) Origin of the electrochemical potential in intercalation electrodes: Experimental estimation of the electronic and ionic contributions for na intercalated into TiS2. *Journal of Physical Chemistry B* 108(41):16093-16099.
24. Zhou X, Wan L-J, & Guo Y-G (2012) Facile synthesis of MoS2@CMK-3 nanocomposite as an improved anode material for lithium-ion batteries. *Nanoscale* 4(19):5868-5871.

25. Wang F, *et al.* (2011) Conversion Reaction Mechanisms in Lithium Ion Batteries: Study of the Binary Metal Fluoride Electrodes. *Journal of the American Chemical Society* 133(46):18828-18836.
26. Gregorczyk KE, Liu Y, Sullivan JP, & Rubloff GW (2013) In Situ Transmission Electron Microscopy Study of Electrochemical Lithiation and Delithiation Cycling of the Conversion Anode RuO2. *Acs Nano* 7(7):6354-6360.
27. Lin F, *et al.* (2014) Phase evolution for conversion reaction electrodes in lithium-ion batteries. *Nature Communications* 5.
28. Halim U, *et al.* (2013) A rational design of cosolvent exfoliation of layered materials by directly probing liquid-solid interaction. *Nature Communications* 4.
29. Wang K, *et al.* (2013) Ultrafast Saturable Absorption of Two-Dimensional MoS2 Nanosheets. *Acs Nano* 7(10):9260-9267.
30. Bao W, *et al.* (2010) Lithography-free fabrication of high quality substrate-supported and freestanding graphene devices. *Nano Research* 3(2):98-102.
31. Liu XH, *et al.* (2012) In Situ TEM Experiments of Electrochemical Lithiation and Delithiation of Individual Nanostructures. *Advanced Energy Materials* 2(7):722-741.

Supplementary Information: Rapid first-cycle lithiation strategy for enhanced performance of Li-MoS_2 batteries as identified by *in situ* studies

Jiayu Wan,[(a),1] Wenzhong Bao,[(a),1,2] Yang Liu[(a),3], Jiaqi Dai[1], Fei Shen[1], Lihui Zhou,[1] Xinghan Cai[2], Dan Urban[1], Yuanyuan Li[1], Katherine Jungjohann,[3] Michael S. Fuhrer*[2,4], Liangbing Hu*[1]
1 Department of Materials Science and Engineering, University of Maryland, College Park, MD 20742-4111, USA.
2 Department of Physics, University of Maryland, College Park, MD 20742-4111, USA.
3 Center for Integrated Nanotechnologies (CINT), Sandia National Laboratories, Albuquerque, New Mexico 87185, United States
4 School of Physics, Monash University, Victoria 3800, Australia.
*Corresponding Authors: binghu@umd.edu, michael.fuhrer@monash.edu
(a) These authors contribute equally to this work

Supplementary Figure S1 (A) shows a image of a $MoS_2/Li_2O/Li$ (positive electrode/electrolyte/negative electrode) nano battery in TEM. After appling a potential difference between the two electrodes, a lithiated product of Li_2S and Mo flake is shown in Figure S2 (B). Supplementary Figure S2 shows an HRTEM image of the final product of Li_2S and Mo. The interconnected network of Mo nanoparticles embeded in a Li_2S matrix can be seen clearly in the image.

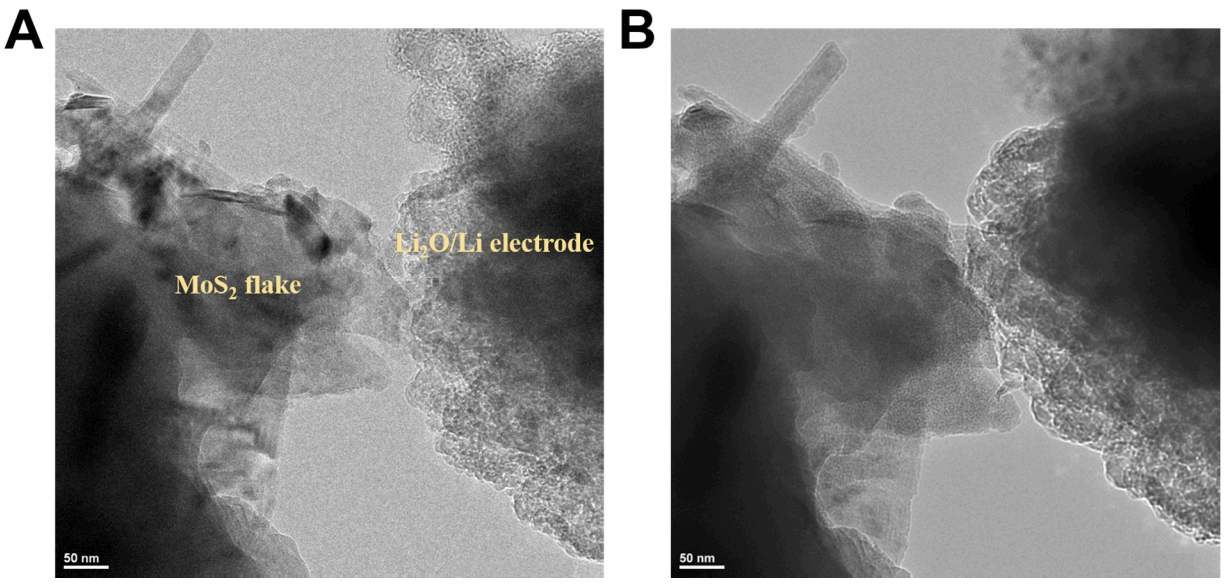

Supplementary Figure S1. Transmission electron micrographs of MoS_2 and Li_xO/Li electrode (A) before and (B) after lithiation of MoS_2.

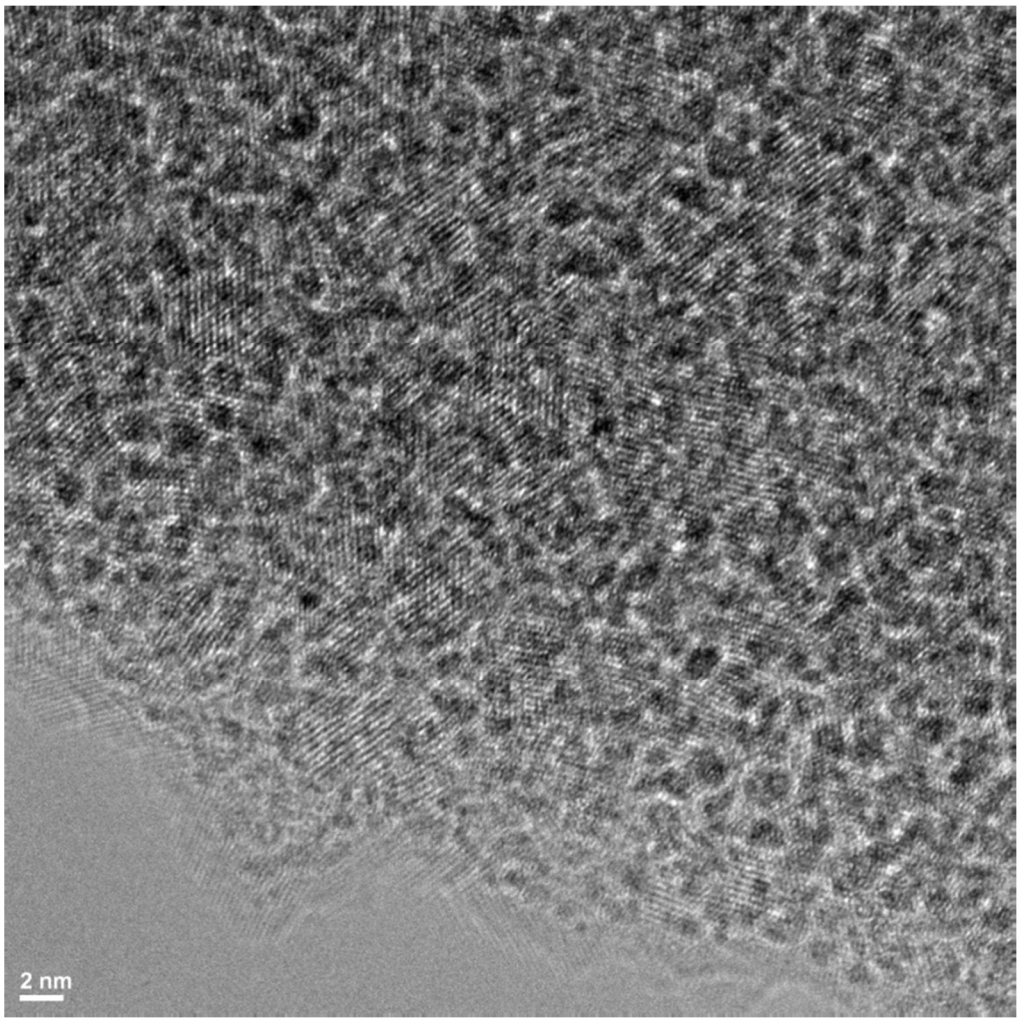

Figure S2. High resolution transmission electron micrograph of MoS_2 flake after lithiation